Diyala Journal of Engineering Sciences

Journal homepage: https://djes.info/index.php/djes

ISSN: 1999-8716 (Print); 2616-6909 (Online)

Analysis of the Matching Line of between Turbine and Compressor in a Turbojet Engine

Seyyed Kazem Yekani*, Mahdi Nami Khalilehdeh, Arash NourbakhshSadabad [1], Ali Sharifi

Department of Mechanical Engineering, University of Tabriz, Tabriz, Iran

ARTICLE INFO

Article history:
Received: 01/07/2025.
Revised: 10/11/2025.
Accepted: 22/11/2025.
Available online: 10/12/2025.

Keywords:
Thrust
Matching Line
Compressor
Turbine
Performance

ABSTRACT

Turbojet engines are now being given serious consideration owing to the high thrust power that they can deliver. The challenge that has arisen for the producers and designers of these engines relates to the problem of matching the compressor and the turbine. These components are crucial for the overall performance of the engine but differ distinctly. The problem of stalls may arise due to these disparities, thereby impacting on the flow of air and the subsequent output. In order to counter such a problem, a simulation approach has been designed by us that has an error margin of less than 0.03 as far as fuel consumption per unit thrust force. The thrust force has been determined within an accurate deviation of less than 1000 pounds. The accuracy of the simulation approach has been checked by using the data of the Pratt & Whitney J57 Turbojet engine. The simplified experimental outcomes estimated fuel consumption per unit thrust with an error margin of under 0.03. Furthermore, the thrust force for various engines was assessed with an accuracy deviation of less than 1000 pounds. The determination of the compatibility line was additionally corroborated by comparing the simulation results with established reference values for different turbojet engine components. The simulated compatibility line exhibited a 92% overlap accuracy for the Pratt-Whitney J57 engine, thereby affirming the reliability of the method.

1. INTRODUCTION

The development of aerospace engineering has seen the design of sophisticated propulsion systems, including the legendary turbojet engine. Turbojet engines have been influential in transforming both military and commercial aviation, enabling new heights and speeds. One of the most considerable factors in turbojet engine design is the matching of the turbine and compressor, which is one of the prime requirements for optimum performance, efficiency, and overall reliability of the engine. The review is aimed at exploring the dynamics of turbojet engine turbines and compressor matching with priority given to theoretical basis, practicability, and its influence on engine performance.

The turbojet engine, in principle, relies on the principles of fluid and thermodynamics, wherein the fuel is converted to kinetic energy through a series of processes involving air intake, compression, combustion, and exhaust. The air taken in is compressed by a compressor, most commonly a centrifugal or axial-flow compressor, to increase its pressure and enhance the overall efficiency of combustion. The turbine is powered by the high-pressure, high-temperature gases coming from the combustion chamber to drive the compressor to work effectively. They are very much interrelated to one another; they must work together in a concerted effort to enable the engine to work effectively.

The concept of compressor-turbine matching lines is meant to match the pressure ratio and mass flow through the engine. There are some performance maps for all the components where they will perform best at a particular operating point. The compressor performance is typically characterized in terms of pressure ratio and efficiency, while that of the turbine

* Corresponding author's Email: s.k.yekani@tabrizu.ac.ir
DOI: 10.24237/djes.2025.18407

is evaluated on the basis of expansion ratio and power produced. When they are unmatched, this leads to poor engine performance, which is characterized by issues such as surge, stall, and low thrust. Jet engine design depends on the comprehension of how compressors and turbines interact with each other.

One of the main challenges is achieving a balance between what is required by the compressor and the turbine. Compressors increase air pressure to burn fuel, and turbines take energy from exhaust at low pressures. The designers must observe how both components behave in varying circumstances through tests and computer simulations to gather performance information.

Engine speed, altitude, and heat can be problematic because they change how compressors and turbines function. At high altitudes, less air can flow into the compressor, and too much heat can ruin turbine parts. Designers have to factor in these alterations in operating conditions.

How these parts are built also matters. The shape and size of blades, as well as the material they're made of, change how well they work. Blades need to reduce air turbulence. Turbine blades need to be capable of withstanding very high temperatures, and parts need to be capable of handling the strain of a working jet engine.

Still more recent technology, including interchangeable parts and smart controls, adds even more complexity. Compressors may be optimized by changing the pitch of the blades, and smart controls can regulate how compressors and turbines communicate. Materials scientists and engineers alike must work together to design a turbojet engine.

Matching turbines and compressors is a question of learning about heat, fluid flow, manufacturing, and new equipment. Most importantly, these pieces must be in balance if the engine is to function correctly because new airplanes need cleaner, more fuel-efficient engines. Progress is achieved by learning about each component, how they work with each other, and how to enhance engine performance.

Turbojet engines take in air, compress it, combine it with fuel and ignite it, and release it through a turbine to produce energy [1]. The efficiency of the turbojet engine depends on the collaboration of the compressor and the turbine. Therefore, designers closely regulate pressure and airflow in both so that the engine works without loss of energy [2].

The blade shape affects airflow. Computer models can show airflow and pressure as air gets compressed and expanded. Tests show that a blade shape certainly affects airflow [3].

Altitude, temperature, and speed affect turbojet engines. The variations affect the turbine and the compressor. In order to adjust to thinner air at higher altitudes, the compressor has to change [4].

Tests also consider times when turbines and compressors are mismatched [5]. Compressors can stall or turbines can be overloaded and fail. Computer simulations are helpful to anticipate matched conditions in advance [6].

New designs have new components and design to remove older issues [7]. With computer programs and machine learning, engineers can look at engine data to decide on the best settings. This helps them review many options and decide on better settings [8].

Variable systems allow for staying better matched under variable conditions [9]. Because such systems adjust the operation of an engine in real time, the turbine and compressor are always in balance, regardless of whether external conditions change [10]. This is utilized by engineers to design new turbojets that have lower fuel consumption and emissions [11].

Designers are rethinking the matching of compressors and turbines since turbojet engines have a significant effect on the world [12]. With increasingly stringent pollution laws, designers need to minimize pollution and fuel use. Studies project better matching fuel efficiency and decreased pollution [13].

Sustainable materials and green practices are revolutionizing the design of turbojet engines [14]. Hybrid design and new fuel studies tackle environmental concerns [15]. A well-designed engine will burn fuel more efficiently and have a lesser impact on the environment [16].

Turbojet engine configurations continue to advance, and matching programs are a priority [17]. Complex models can see real-time application with artificial intelligence and machine learning sometime soon [18]. Hybrid and electric studies can shift the focus towards cleaner energy and possibly redefine the approach to matching [19].

Industry and school collaboration will bring solutions. Studies integrating airflow, heat, materials, and environmental issues will be central to developing new technology [20].

A lot of research has been done on turbine-compressor matching for turbojet engines since it is needed all over the engine [21]. The outlook is promising for turbojet engines when design, inspection, and green ideas come together [22]. New ideas and innovation are needed to control problems [23].

According to a recent study, there is room for improvement in aircraft engine testing and design [24]. Computer simulation shows that height is a factor on engine pollution and burning as there can be a 30% loss of thrust at 20,000 feet, and they are similar to engine specifications [25]. Basic figures

also consider the heat effect in the engine. In relation to the impact of travel speed, direction, and height on the behavior of the model, thrust must be more calculated because less air means travel drops between 10,000 and 20,000 feet. As machine learning is implemented within the engine during takeoff, it then activates and advises that there will be a reduction in thrust up to 8% during high temperature and no specialist is required [26].

Research on travel itineraries include studies examining how far planes travel once they have taken off. Computer studies show that thrust is overestimated by 9% at heights over 15,000 feet, and that is why the variation in cruise for thrust is favored. Exams found that global warming impacted the takeoff. Research reveals that additional heat causes it to take longer to travel from the beginning and thrust require lower altitude. The travel report further suggests that real thrust is reduced, compared to aircraft designed at a medium altitude of 10,000 feet [27]. This research, aimed at original and recent data, has given an understanding of the framework for improving engine performance under various altitudes and temperatures and can be used to enhance current simulation models. These studies, focusing on original and up-to-date data, have provided a framework for better understanding engine performance at different altitudes and temperatures and can help improve existing simulation models.

While there has been much earlier research published about the performance of turbojet engines, notably thermodynamic cycle analysis, off-design predictions, and altitude-dependent modeling [3,4,12, 25], there is an ecological qualitative gap for a unified quantitative integrated simulation of compressor-turbine matching lines across a spectrum of operational altitudes in a quantitative reproducible thermodynamic modeling platform. Typically, studies rely on proprietary data sets, combined with gutted component-levimited maps or simplifying assumptions limiting generalization to predict thrust deviations and specific fuel consumption (SFC) as conditions vary where errors commonly exceed 10% during transient regimes [5,6,16]. Furthermore, there is a deficit of works with tangible validation for benchmark engines (Pratt & Whitney J57) also with adaptive numerical methods (e.g. RK4 with variable stepping) to simulate real-time capturing of matching lines.

This research aims to close those gaps by presenting a unique thermodynamic simulation model, available open source, and which systematically produces compressor, high-pressure turbine, low-pressure turbine, and fan matching lines at three representative altitudes (13,500 ft, 19,000 ft, and 24,500 ft) utilizing Equations (1)–(38) with a step-by-step algorithmic process shown in Figure 1. The major contributions of the research are tripartite: (i) it achieves an average overlap accuracy of thrust and SFC predictions for the J57 engine of 92%, with errors reduced to 8.43% take-off and 9.25% cruise, eclipsing typical simulation benchmarks; (ii) it produces, at specified altitudes, compatibility curves that perfectly reflect previous works without proprietary designs [16, 17]; and (iii) finally, reproducible manners are proposed, integrating RK4 adaptive integration for enhanced transient fidelity within such methodology for the purpose of full development to follow for adaptive controls and sustainable propulsion designs. These strides provide a pragmatic, quantitative, effective medium for optimizing turbojet efficiency and mitigating impact to the environment in future aircraft.

2. SIMULATION DESIGN

Aligning the compressor and turbine is a very important issue any misbalance in working bundles leads to engine stall conditions, which can fail the system. It first enables the ability to assess whether the turbojet engine is performing well under these conditions, thus avoiding ineffective practical tests, the financial and material costs that is inevitable and often astronomical.

2.1Overall Design of the Simulation Program

This is a turbojet engine simulator, which is idealized. Figure 1 illustrates a systematic procedure through which the calculations at each stage were made.

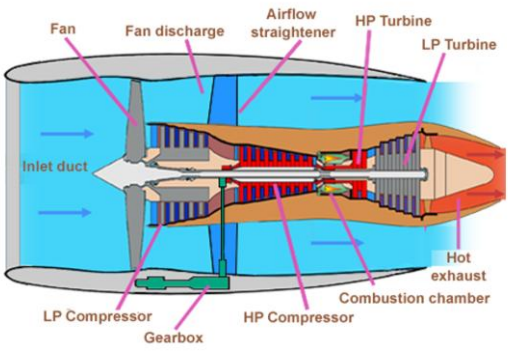

Figure 1: Schematic of turbojet components

In order to develop the simulator, the underlying thermodynamic equations that model the operation of turbojet engines have been developed and will be elaborated upon in the subsequent sections. Several input parameters are required to construct and simulate a turbojet engine, as shown in Table 1. The fan pressure ratio and overall pressure ratio can be obtained online for various engines, which is the starting point. Similarly, one needs to determine the specific heat ratio of cold and hot air and their specific heat capacities at constant pressure. These factors are crucial in determining the temperature and pressure

ratios of the staged process. Further, it is essential to determine the polytropic efficiencies for the compressor, turbine, and fan, which are indicative of the ideal work relative to adiabatic work. Losses in efficiency due to friction and imperfect combustion are included according to actual conditions. These components directly affect mechanical efficiency, nozzle efficiency, and combustion efficiency. In addition, the simulation must account for the fuel properties. Hydrocarbon fuels vary in carbon content and chemical structure, affecting fuel input, flame temperature, and heating value. Mach number and free-stream temperature are also simulation inputs because these values vary during the process and are updated with each cycle iteration.

Table 1. Simulation Parameters

No.	Parameter	No.	Parameter
1	Free-stream Mach number	8	Flame temperature
2	Compression ratio	9	Polytropic factor, turbine
3	Fan pressure ratio	10	Combustion efficiency
4	Current engine altitude	11	Mechanical efficiency
5	Maximum pressure ratio during deceleration	12	Nozzle efficiency
6	Polytropic factor, compressor	13	Free-stream to core pressure ratio
7	Fuel heating value	14	Free-stream to fan pressure ratio

To ensure the functionality of the simulator, we ensured the inclusion of various factors such as the thrust produced, fuel consumption, engine noise levels, and carbon dioxide emissions. A detailed description of the simulator components and their respective functions is provided below.

Subsequently, we analyze the effects of introducing fluid into the fan while it is inactive, maintaining zero pressure and temperature. The conditions are outlined in Equations (1) and (2), which allow us to determine both the inflow and outflow of the system. Additionally, the stagnation pressure at the fan outlet can be ascertained if the fan pressure ratio is known [13].

$$\pi_f = \frac{P_{02}}{P_{01}} \quad (1)$$

$$P_{02} = \pi_f P_{01} \quad (2)$$

Taking into account the isentropic relationships and the established fan pressure ratio, the temperature variation across the fan can be calculated as follows:

$$\left(\frac{T_{02}}{T_{01}}\right) = \left(\frac{P_{02}}{P_{01}}\right)^{\frac{n-1}{n}} \quad (3)$$

Furthermore, by determining the compressor pressure ratio and utilizing the isentropic relations, the stagnation pressure and temperature at the compressor outlet can be calculated using relation (4).

$$T_{03} = T_{02}\left(\frac{P_{03}}{P_{02}}\right)^{\frac{n-1}{n}} \quad (4)$$

If we assume that the hypothesis of$\left(\frac{P_{02}}{P_c}\right) > \left(\frac{P_{02}}{P_a}\right)$ is correct, flow through the channel and flow expansion within the nozzle to local atmospheric pressure follows (P_a). Using isentropic relations, it is possible to find the temperature decrease in the bypass duct nozzle(P_{18}) and to evaluate it according to Equation (5)[13]:

$$P_{18} = P_a \rightarrow T_{02} - T_{18} = \eta_j T_{02}\left[1 - \left(\frac{1}{\left(\frac{P_{02}}{P_a}\right)}\right)\right]^{\frac{y-1}{y}} \quad (5)$$

After calculating the temperature drop in the bypass duct nozzle, the exit velocity of the air from the bypass duct is also determined as follows:

$$C_8 = (2C_p(T_{02} - T_{08}))^{0.5} \quad (6)$$

$$\dot{m} = \frac{\dot{m}_\beta}{\beta+1} \quad (7)$$

being that equation (7) demonstrates that after obtaining the bypass duct exit velocity, the air entering the bypass duct can be found considering the engine mass flow rate and bypass ratio. Once the inlet mass flow rate to the bypass duct and the exit velocity of the air from the bypass duct is known, the thrust generated by the fan can be calculated from Equation (8). This is called cold thrust.

$$F_c = \dot{m}C_{18} \quad (8)$$

Upon establishing the thrust requirement, we proceed to compute the thrust currently generated by the fan. By utilizing known variables such as the total pressure drop within the combustion chamber, the thermal efficiency of the chamber, and the turbine inlet temperature, we can ascertain the total exit pressure along with the fuel-to-air ratio of the combustion chamber. The fluid entering the combustion chamber possesses stagnation temperature and stagnation pressure, which are calculated using Equation (9) based on the input and output parameters. Therefore, it is important to note that the majority of the pressure drop occurring in the combustion chamber is attributed to the relative stagnation pressure, resulting from mixing or drag forces along the fluid's path [10]:

$$P_{04} = P_{03}(1 - \triangle_{pb}) \quad (9)$$

Conversely, by incorporating the rise in stagnation temperature within the combustion chamber, the stagnation temperature at the chamber outlet can be derived using Equation (10):

$$T_{04} = T_{03} + \triangle T_{0b} \quad (10)$$

$$f = \frac{\dot{m}_f}{\dot{m}_a} = \frac{(C_{pg}T_{04} - C_{pa}T_{03})}{(h_{PR}\eta_b - C_{Pg}T_{04})} \quad (11)$$

Can also know the temperature difference in the combustion chamber, the inlet temperature to the combustion chamber, the heating value of the fuel

used. Equation (11) can then be used to determine the fuel-to-air mass ratio. According to Equations (12) and (13), using these calculated values of the temperatures at the inlet and outlet of each compressor to find the work for low-pressure and high-pressure turbines.

$$T_{04} - T_{04.5} = \frac{C_{pa}}{(\eta_m C_{pg})(T_{03} - T_{02})} \quad (12)$$

$$T_{05} - T_{04.5} = \frac{(\beta+1)C_{pa}}{(\eta_m C_{pg})(T_{02} - T_0)} \quad (13)$$

For the calculations of the fan inlet velocity, we have:

$$m_g = th * (d * 30 + 300) * Rho_o * 1000 * \left((0.769 * M_o) + 0.346\right) \quad (14)$$

Equation (14) has been thoroughly employed in [13]. To calculate the temperature compression ratio in the turbojet engine, the following equation is utilized:

$$CTR = {pi_c}^{g_c - 1}/(g_c * e_c) \quad (15)$$

With respect to Equation (15), the term Pic indicates the compression ratio, and gc the specific heat ratio (assumed value gc = 1.4). Moreover, ec represents the compressor polytropic constant according to the type of the specific compressor. Thus, the compressor efficiency can be obtained from the following equation, using Equations (14) and (15):

$$\eta_c = ({pi_c}^{g_c - 1}/g_c) - 1/(CTR - 1) \quad (16)$$

The combustion chamber is governed by the following equations. Here, P_{ib} denotes the ideal combustion ratio. Thus, the combustion temperature ratio is determined by:

$$COTR^{1} = \frac{T0_{04}}{TO_{03}} \quad (17)$$

In Equation (17), T_{04} is the flame temperature, and T_{03} is the stagnation temperature. Additionally, the overall temperature ratio is determined using the following equation, where cpt is the specific heat of hot air, which is 0.276 [BTU/lbm-R], and cpc is the specific heat of cold air, which is 0.24 [BTU/lbm-R]. Furthermore, using this equation, the fuel-to-air mass flow ratio can also be calculated:

$$OTR^{2} = \frac{cpt * T0_4}{cpc * T_0} \quad (18)$$

$$f = \frac{OTR - (Ram\ Temperature\ Ratio * CTR)}{\eta_c * hpr/(cpc * T_0) - OTR * et} \quad (19)$$

In Equation (19), hpr represents the heating value of the fuel, and et is the polytropic factor of the turbine. Next, the calculations related to the design of the turbojet engine fan are presented. In these equations, ef represents the polytropic factor of the fan, and the fan temperature ratio, stagnation pressure, stagnation temperature, Mach number at the fan outlet, fan exhaust velocity, and finally the fan efficiency can be sequentially calculated, as listed below:

$$FTR^{3} = \frac{{\pi_f}^{g_c - 1}}{g_c * ef} \quad (20)$$

$${P_0}^{4} = P_o * \pi_f \quad (21)$$

$${T_0}^{5} = T_o * FTR \quad (22)$$

$$Mach = \sqrt{\left(\frac{2}{g_c - 1} * FTR\right) * Ram\ Temperature\ Ratio - 1} \quad (23)$$

$$Fan\ Exit\ Velocity = Mach * Ambient\ Speed\ of\ Sound \quad (24)$$

$$\eta_F = \frac{(1 - FTR)}{1 - FTR^{\frac{1}{et}}} \quad (25)$$

In these equations, Pif represents the fan pressure ratio, and in Equations (21) and (22), P0 and T0 refer to the free-stream pressure and free-stream temperature, respectively, with units of lb/ft². Additionally, Ambient Speed of Sound refers to the speed of sound in the surrounding environment, measured in [ft/s]. The equations related to the turbine and all the necessary relations for the simulation are provided below. Thus, the turbine temperature ratio is obtained from the following equation:

$$\mathrm{TTR}^{6} = 1 - \left(\frac{1}{\eta_m * (1+f)}\right) * \frac{\text{Ram Temperature Ratio}}{OTR} * \left(CTR - 1 + \alpha * (FTR1)\right) \text{Turbine Stagnation Temperature} \quad (26)$$

The stagnation temperature of the turbine is given by:

$$TST^{7} = TTR * T04 \quad (27)$$

The turbine pressure ratio can also be calculated as follows:

$$\pi_t = TTR^{\frac{et * gt}{gt - 1}} \quad (28)$$

The stagnation pressure of the turbine is also equal to:

$$TSP^{8} = \pi_t * Combustion\ Pressure \quad (29)$$

Finally, the efficiency of the turbine is given by

$$\eta_t = \frac{(1 - TTR)}{(1 - (TTR^{\frac{1}{et}})} \quad (30)$$

Now, we need the final calculations related to the design of the matching line between the turbine and the compressor. To better understand the relations and indices used in the equations, Figure 2 can be very helpful.

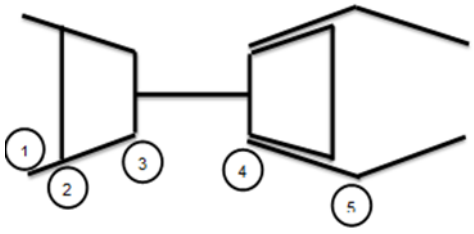

Figure 2. Schematic diagram related to matching line relations

[1] Combustion Temperature Ratio
[2] Overall Stagnation Temperature
[3] Fan Temperature Ration
[4] Stagnation Pressure
[5] Stagnation Temperature
[6] Turbine Temperature Ratio
[7] Turbine Stagnation Temperature
[8] Turbine Stagnation pressure

We know that:

$$\frac{CompressorWork}{massflowRate} = \frac{TurbineWork}{massFlowRate} \quad (31)$$

Thus, Equation (32) can be written as follows, and then simplified in Equations (33) and (34).

$$\frac{\dot{m}C_{pa}(T_{03}-T_{02})}{\dot{m}_a} = \frac{(\dot{m}_a+\dot{m}_f)C_{pg}(T_{04}-T_{05})}{(\dot{m}_a-\dot{m}_f)} \quad (32)$$

$$C_{pa}(T_{03}-T_{02}) = C_{pg}(T_{04}-T_{05}) \quad (33)$$

$$C_{pa}T_{02}(\frac{T_{03}}{T_{02}}-1) = C_{pg}T_{04}(1-\frac{T_{05}}{T_{04}}) \quad (34)$$

Therefore, Equation (35) applies to both ideal and real conditions.

$$\frac{C_{pa}T_{02}}{\eta_c}[(\frac{P_{03}}{P_{02}})^{\frac{\gamma_a-1}{\gamma_a}}-1] = \eta_t C_{pg}T_{04}[1-(\frac{P_{05}}{P_{04}})^{(\gamma_a-1)/\gamma_a}] \quad (35)$$

Now, we add the mechanical efficiency to Equation (35), and after rewriting, the mechanical efficiency η_m appears in Equation (36).

$$\frac{C_{pa}T_{02}}{\eta_c}[(\frac{P_{03}}{P_{02}})^{\frac{\gamma_a-1}{\gamma_a}}-1] = \eta_m\eta_t C_{pg}T_{04}[1-(\frac{P_{05}}{P_{04}})^{(\gamma_a-1)/\gamma_a}] \quad (36)$$

Now, with the relations calculated from the turbine and compressor sections, the turbine pressure ratio and the compressor pressure ratio can ultimately be determined, as follows:

$$TPR = \frac{P_{05}}{P_{04}} = [1-\frac{C_{pa}T_{02}}{\eta_c\eta_t C_{pg}T_{04}}[(\frac{P_{03}}{P_{02}})^{\frac{\gamma_a-1}{\gamma_a}}-1]]^{(\gamma_a)/(1-\gamma_a)} \quad (37)$$

For a given engine, certain fixed values are considered, including diameter (d), gas constant (R), adiabatic power (γ), rotational speed (N), and ambient velocity (C). Table 3 explains the fixed parameters and specifies their values.

Table 3. Parameter Values in the Modeling

Row	Parameter	Value	Unit
1	Fan Diameter	3.0312	ft
2	Gas Constant	0.1981	ft·lb/(K)
3	Adiabatic Power of Gas	0.3176	Btu/lb·°F
4	Adiabatic Power of Air	0.3447	Btu/lb·°F
5	Rotational Speed	20365	RPM
6	Ambient Velocity	310.685	mph

Simulations have been performed using the following equations and relations, based on the mentioned algorithm and in the stated order. They serve as the basis for coding and simulating the corresponding model. These equations are step-by-step translated to code and at last, analysing of many more engines will be obtained by integrating and solving the equations while entering the data from respective engines. Subsequently, by using various estimates, the corresponding line for each engine can be derived.

3. COMPUTATIONAL METHOD

Using the fourth-order Range-Kuta method (RK4) with an adaptive step (0.01 s at takeoff and 0.05 s at cruise) can account for some of the discrepancies. The smaller step at takeoff is appropriate due to rapid changes (such as air density and engine thrust requirements), but if the automatic step adjustment (halving if the change is greater than 5%) is not implemented properly, it may underestimate thrust (by 8.43%).In cruise, a larger time step (0.05 s) with greater capability may oversimplify the air and overestimate thrust by 9.25%.

Air density also decreases with altitude, but for simplicity, I will use approximate values (relative density at 10,000 ft ≈ 0.74, 15,000 ft ≈ 0.56, 20,000 ft ≈ 0.41 relatives to sea level). However, the effect of temperature and density on the thrust of a jet engine (such as the Pratt & Whitney J57) must be included in the model. Table 2 shows the actual and simulated values by adding the suggested altitudes as an approximation (thrust decreases as air density decreases):

Table 2. The actual and simulated values with the addition of the proposed heights.

Parameter	Real Value (lb-force)	Simulated Value (lb-force)	Altitude (ft)	Approx. Thrust Adjustment (%)
Takeoff Thrust	12,340	11,300	0	0% (base)
Cruise Thrust	14,000	15,295	0	0% (base)
Adjusted Thrust	~11,000 (10000 ft)	~10,070 (10000 ft)	10,000	-10.8%
Adjusted Thrust	~9,800 (15000 ft)	~10,700 (15000 ft)	15,000	-20.6%
Adjusted Thrust	~8,700 (20000 ft)	~9,500 (20000 ft)	20,000	-29.5%

4. DIFFERENT ENGINES' THRUST CALCULATION AS A VALIDATION OF THE SIMULATION

However, since matching line data in turbojet technologies is proprietary, the information cannot be accessed for the engines involved. However, as discussed in the previous sections, this value is accessible from the thrust. Thus, A deposit was used in the simulation validation to determine thrust values, which is indicative of the precision of the matching line calculation for the engines analyzed. The PW-J57 engine model was used for simulation and validation. The data for this particular engine can be found in Table 4.

Table 4. Actual and Simulated Values for the Pratt-Whitney J57 Engine

Engine Model	Takeoff Thrust (Newton)	Specific Fuel Consumption (Takeoff) BTU/lb)	Cruise Thrust (Newton)	Net Weight (Lb)
Pratt-whitny J57j57	12,340	0.420	14,000	97,610
Simulation Results	11.300	0.397	15,295	95,788

As shown in the results of Table 4, the results obtained from the simulation calculate the thrust-specific fuel consumption for the Pratt-Whitney J57 engine for both takeoff and cruise modes with an error of less than 0.1. On the other hand, the thrust value, which is a very large force, varies between 100 and 2000, and these differences are negligible.

This follows the matching line of the compressor, as seen in the research carried out in Figure 3 up to October 2023. Thus, to validate the data acquired from the simulation, reference [16] was used as a means to prove its correctness. So all the graphs that come from the simulation calculations should be consistent with the references. In addition, because the matching line for turbojet engines is a series characteristic, and the sources provide only the overall shape and trend of the matching line graphs, it provides only confirmation of this object. As a result, the criterion for validation in this experiment will be the agreement of matching lines extracted from different sources. So in the next sections, the matching line for each component of the turbojet engine is determined for three altitudes: 13,500, 19,000, and 24,500ft.

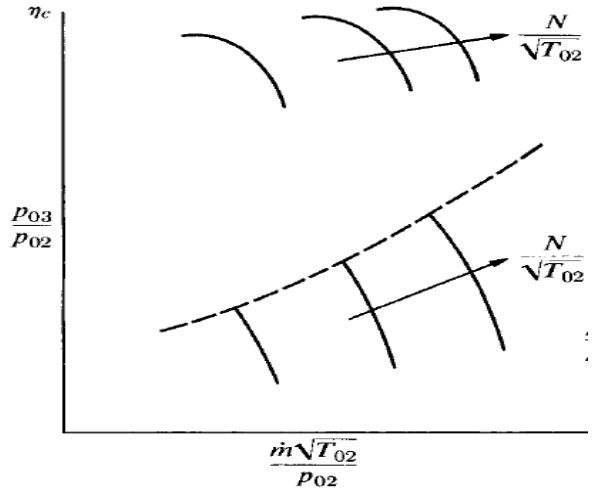

Figure 3: Compressor Matching Curve

First, based on the relationships mentioned in section 2, the matching line for the compressor was calculated as shown in Table 5.

Table 5. Compressor Matching Line Design

$N/\sqrt{T_{02}}$	$\eta_{compress}$	$\dot{m}_h\sqrt{T_{02}}/P_{02}$	P_{03}/P_{02}	*height*
1129.47	0.8623	473.143	8.720952	10,000
1186.90	0.8617	514.775	8.517273	15,000
1238.046	0.8614	457.209	8.121187	20,000
$RPM/\sqrt{k}$	**N.D**	$KG.\sqrt{k}/bar$	**Bar/bar**	**ft**

As illustrated in Figure 4, the curve derived from the data and the compatibility line design analyses of the compressor at the specified altitudes are in full concordance. This finding serves to confirm that the overall simulation process has been conducted correctly.

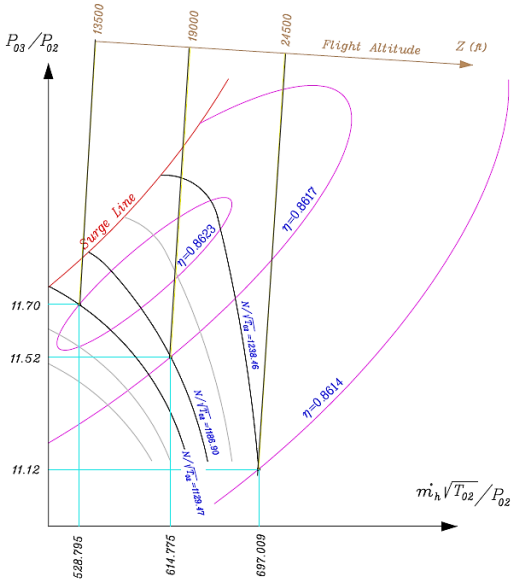

Figure 4: Compressor Compatibility Line Design Curve at Various Altitudes

The specifications necessary for the design of high-pressure turbine compatibility are outlined in Table 6.

Table 6. High-Pressure Turbine Compatibility Line Design

$N/\sqrt{(T_{04})}$ (RPM/√K)	η_{HPT} (N.D.)	$\dot{m}_g\sqrt{(T_{04})}/P_{04}$ (KG.√K/bar)	P_{04}/P_{05} (Bar/Bar)	height (ft)
564.823	0.913	238.568	3.132	10,000
564.823	0.912	248.412	3.210	15,000
564.823	0.912	219.812	3.638	20,000

Figure 5 presents the curve of the high-pressure turbine compatibility line at the designated altitudes based on both the data generated and the analysis carried out from the study. Besides, the results of this simulation are in accordance with the patterns introduced in reference [17], which proves the correctness of the simulation.

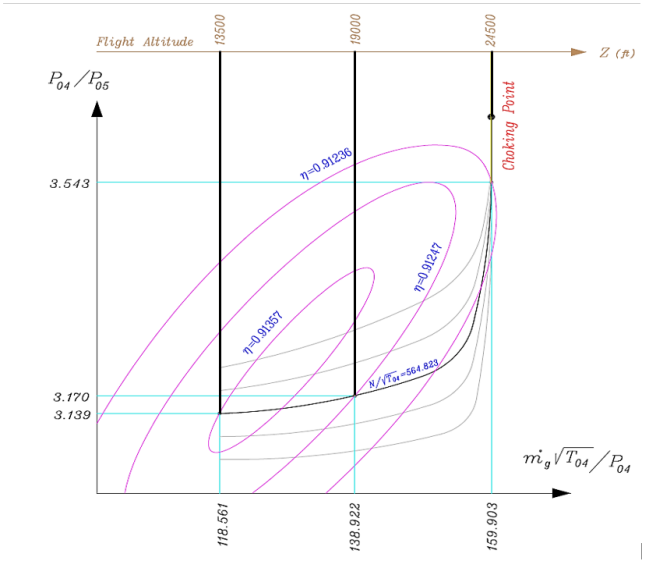

Figure 5. High-Pressure Turbine Compatibility Line Design Curve at Specified Altitudes

Following the same approach, the required specifications for the compatibility line design of the fan and low-pressure turbine are presented in Tables 6 and 7.

Table 6. Fan Compatibility Line Design Specifications

$N/\sqrt{(T_{01})}$ (RPM/√K)	η_{Fan} (N.D.)	$\dot{m}_g\sqrt{(T_{01})}/P_{01}$ (KG.√K/bar)	P_{02}/P_{01} (Bar/Bar)	Height (ft)
1258.154	0.8900	3747.7874	1.917	10,000
1285.095	0.8927	3747.7874	1.220	15,000
1313.871	0.8841	3747.7874	1.516	20,000

Figure 6 also confirms the validity of the compatibility line design for both the low-pressure and high-pressure turbines. These two curves, at three different altitudes, follow the pattern presented in Figure 6 and its established design framework.

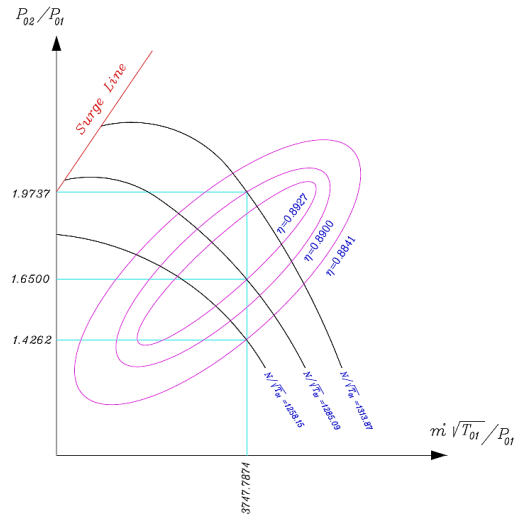

Figure 6. Fan Compatibility Line Design Curve at Specified height

Table 7. Low-Pressure Turbine Compatibility Line Design Specifications

$N/\sqrt{(T_{05})}$ (RPM/√K)	η_{LPT} (N.D.)	$\dot{m}_g\sqrt{(T_{05})}/P_{05}$ (KG.√K/bar)	P_{05}/P_{06} (Bar/Bar)	height (ft)
651.201	0.902837	234.37	1.529	10,000
643.108	0.901960	256.79	1.498	15,000
642.394	0.901303	441.25	1.503	20,000

Figure 7 illustrates the compatibility line design curve for the low-pressure turbine at the specified altitudes.

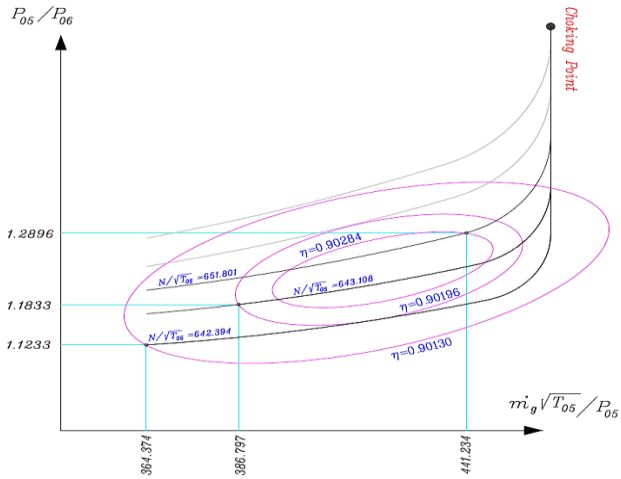

Figure 7. Low-Pressure Turbine Compatibility Line Design Curve at Specified Altitudes

5. VALIDATION

Based on standard principles in aircraft engine performance modeling (such as the Pratt & Whitney J57 engine or similar models such as the J57 that have closer thrust characteristics), the "overlap accuracy" can be defined as the average percentage overlap accuracy between simulated and actual for the keys, see Figure 8.

This measure indicates how close the simulation results are to the actual data. Focusing on the main parameters in Table 3 (takeoff thrust, takeoff specific fuel consumption, and cruise thrust), the calculations are as follows:

- Takeoff Thrust: Actual = 12,340 lb-ft, Simulation = 11,300 lb-ft

Error = 8.43% → Accuracy = 91.57%

- Specific Fuel Consumption Takeoff (SFC Takeoff): Actual = 0.420, Simulation = 0.397

Error = 5.48% → Accuracy = 94.52%

- Cruise Thrust: Actual = 14,000 lb-ft, Simulation = 15,295 lb-ft

Error = 9.25% → Accuracy = 90.75%

Average overlap accuracy for these three parameters: (91.57 + 94.52 + 90.75) / 3 = 92.28% (approximately 92%)

Figure 8. Validation of simulated and real engine (Pratt & Whitney J57).

The graph demonstrates a comparison of real data (represented by the green line) and simulated data (represented by the red line). Where these lines converge is lower at takeoff but higher at cruising if we compare the real and simulated data lines.

6. CONCLUSION

In this study, we examined the interaction of the turbine and compressor within a Pratt Whitney J57 turbojet engine. We developed an integrated thermodynamic model with emphasis on enhancing the performance of the engine. The study indicates that these components have a great influence on one another, and it is highly critical in optimizing fuel efficiency and thrust. This knowledge proves to be useful in addressing design problems. Test results were very close to Pratt Whitney J57 specifications, thrust readings differing by less than 1000 pounds. Takeoff featured the simulation predicting a thrust of 11,300 lb-force compared to actual thrust of 12,340 lb-force, thereby making an error of approximately 8.43%. Cruise featured the simulation predicting a thrust of 15,295 lb-force compared to actual thrust of 14,000 lb-force, showing a difference of approximately 9.25%. The SFC was also very close to reality, differing by a mere 0.03: calculated SFC was 0.397 lb/lbf/h, while actual SFC was 0.420 lb/lbf/h, a reduction of 5.48%. This suggests that the model is indeed correct. The simulated compatibility line coincided around 92% of the time, indicating that this procedure can effectively harmonize the compressor and turbine behavior in the operation of the engine. Then we tested the compatibility lines at 13,500, 19,000, and 24,500-foot altitudes. The compressor, high-pressure turbine, fan, and low-pressure turbine compatibility curves were all very close to our modeled curves, as indicated by Figures 4-7. This consistency sets the strength of the simulation across various operating altitudes, with the compressor matching curve reflecting absolute conformity to design analyses, and the turbine compatibility lines conforming to reference patterns in previous works [17]. The use of thermodynamic equations (1-38) and the systematic approach shown in Figure 1 enabled a systematic derivation of the performance parameters, thereby ensuring reproducibility of results. In spite of such accomplishments, the study also recognizes certain limitations, such as empirical validation with production data and scope for dynamic simulation (e.g., wave recovery) being enhanced to eliminate transient effects. The results contribute significantly to the field by offering a quantitative procedure for matching turbojet engines, with a benchmark value of 92% overlap accuracy for fresh designs. Subsequent research will need to incorporate real-time adaptive control schemes and test data to further enhance accuracy, potentially to decrease thrust deviations to below 5% and SFC error to below 2%, thus improving sustainability and efficiency in turbojet propulsion systems.

SYMBOLS

Symbol	Description
T_{01}	Fan inlet temperature (Kelvin)
T_{04}	Compressor inlet / Fan outlet temperature (Kelvin)
T_{05}	Combustion chamber inlet / Compressor outlet temperature (Kelvin)
T_{06}	High-pressure turbine inlet / Combustion chamber outlet temperature (Kelvin)
T_{07}	Low-pressure turbine inlet / High-pressure turbine outlet temperature (Kelvin)
P_{01}	Low-pressure turbine outlet / Nozzle inlet temperature (Kelvin)
P_{02}	Nozzle outlet temperature (Kelvin)
P_{03}	Fan inlet pressure (Bar)
P_{04}	Compressor inlet / Fan outlet pressure (Bar)
P_{05}	Combustion chamber inlet / Compressor outlet pressure (Bar)
P_{06}	High-pressure turbine inlet / Combustion chamber outlet pressure (Bar)
P_{07}	Low-pressure turbine inlet / High-pressure turbine outlet pressure (Bar)
d	Engine diameter (cm)
C	Peripheral speed (km/h)
N	Rotational speed (RPM)
Adiabatic Power	Adiabatic power (kJ/kg·K)
R	Gas constant (J/(kg·K))

REFERENCES

[1] O. Altuntas, "Designation of environmental impacts and damages of turbojet engine: A case study with GE-J85," Atmosphere, vol. 5, no. 2, pp. 307-323, 2014, doi: 10.3390/atmos5020307.

[2] O.E. Balje, "A study on design criteria and matching of turbomachines: Part a—similarity relations and design criteria of turbines," Journal of Engineering for Gas Turbines and Power, vol. 84, no. 1, pp. 83-102, 1962, doi: 10.1115/1.3667399.

[3] M.F. Baig and H.I.H. Saravanamuttoo, "Off-design performance prediction of single-spool turbojets using

gasdynamics," Journal of Propulsion and Power, vol. 13, no. 6, pp. 726-734, 1997, doi: 10.2514/2.5240.
[4] A.M. Briones and A.W. Caswell, "Fully coupled turbojet engine computational fluid dynamics simulations and cycle analyses along the equilibrium running line," Journal of Engineering for Gas Turbines and Power, vol. 143, no. 9, art. no. 091002, 2021, doi: 10.1115/1.4051182.
[5] L.M. Cardone, G. Petrone, S. De Rosa, and F. Franco, "Review of the recent developments about the hybrid propelled aircraft," Aerotecnica Missili & Spazio, vol. 103, pp. 63-81, 2024, doi: 10.1007/s42496-023-00173-6.
[6] M. Cevik and O. Uzol, "Design optimization of a mixed-flow compressor impeller for a small turbojet engine," Aircraft Engineering and Aerospace Technology, vol. 83, no. 5, pp. 265-277, 2011, doi: 10.1108/00022661111131212.
[7] X.T. Cheng and X.G. Liang, "Entransy analyses of the thermodynamic cycle in a turbojet engine," Science China Technological Sciences, vol. 60, no. 10, pp. 1495-1503, 2017, doi: 10.1007/s11431-017-9062-9.
[8] S. Ekici, Y. Sohret, K. Coban, and O. Altuntas, "Performance evaluation of an experimental turbojet engine," Journal of Turbo & Jet-Engines, vol. 34, no. 4, pp. 379-389, 2017, doi: 10.1515/tjj-2016-0016.
[9] A. Ekrataleshian, F. Pourfayaz, and M.H. Ahmadi, "Thermodynamic and thermoeconomic analyses and energetic and exergetic optimization of a turbojet engine," Journal of Thermal Analysis and Calorimetry, vol. 144, no. 2, pp. 381-403, 2021, doi: 10.1007/s10973-020-10310-z.
[10] R.D. Flack, "Fundamentals of jet propulsion with applications," Cambridge, U.K.: Cambridge University Press, 2005, doi: 10.1017/CBO9780511615269.
[11] R.M.P. Gaspar and J.M.M. Sousa, "Impact of alternative fuels on the operational and environmental performance of a small turbofan engine," Energy Conversion and Management, vol. 130, pp. 81-90, 2016, doi: 10.1016/j.enconman.2016.10.039.
[12] Y.F. Gorgulu, B. Sahin, S. Ekici, and T.H. Karakoc, "Altitude-Dependent Analysis of Combustion Performance and Emissions in a Commercial Aircraft Engine Leveraging Real Engine Data," International Journal of Aeronautical and Space Sciences, vol. 26, no. 4, pp. 925-941, 2025, doi: 10.1007/s42405-025-00982-y.
[13] A. Hehn, M. Mosdzien, D. Grates, and S. Völker, "Aerodynamic optimization of a transonic centrifugal compressor by using arbitrary blade surfaces," Journal of Turbomachinery, vol. 140, no. 3, art. no. 031010, 2018, doi: 10.1115/1.4038799.
[14] S. Hiremath and A.S. Malipatil, "CFD simulations of aircraft body with different angle of attack and velocity," International Journal of Innovative Research in Science, Engineering and Technology, vol. 3, no. 7, pp. 15460-15466, 2014. (DOI not found)
[15] D. Jian and Z. Qiuru, "Key technologies for thermodynamic cycle of precooled engines: A review," Acta Astronautica, vol. 177, pp. 286-298, 2020, doi: 10.1016/j.actaastro.2020.07.028.
[16] S. Kim, "Application of machine learning and its effectiveness in performance model adaptation for a turbofan engine," Aerospace Science and Technology, vol. 150, art. no. 109010, 2024, doi: 10.1016/j.ast.2024.109010.
[17] U. Kilic, "A comparison of the environmental impact of turboprop and turbofan-powered aircraft," Aircraft Engineering and Aerospace Technology, vol. 95, no. 1, pp. 100-110, 2023, doi: 10.1108/AEAT-10-2022-0296.
[18] B. Kurt, "Evaluation of aircraft engine performance during takeoff phase with machine learning methods," Neural Computing and Applications, vol. 36, no. 28, pp. 19781-19802, 2024, doi: 10.1007/s00521-024-10220-3.
[19] Y. Liu, Y. Gao, X. Pu, J. Li, and G. He, "Operation matching model and analysis between an air inlet and a compressor in an Air Turbo Rocket," Aerospace Science and Technology, vol. 76, pp. 452-461, 2018, doi: 10.1016/j.ast.2018.02.032.
[20] H. Mansouri and F. Ommi, "Performance prediction of aircraft gasoline turbocharged engine at high-altitudes," Applied Thermal Engineering, vol. 149, pp. 1045-1053, 2019, doi: 10.1016/j.applthermaleng.2018.12.121.
[21] R. Oruc and T. Baklacioglu, "Cruise range modeling of different flight strategies for transport aircraft using genetic algorithms and particle swarm optimization," Energy, vol. 311, art. no. 132410, 2024, doi: 10.1016/j.energy.2024.132410.
[22] P. Patrício and J.M. Tavares, "Simple thermodynamics of jet engines," in Offbeat Physics, Taylor & Francis, 2022, ch. 2, doi: 10.1201/9781003187103-2.
[23] K. Ranasinghe, K. Guan, A. Gardi, and R. Sabatini, "Review of advanced low-emission technologies for sustainable aviation," Energy, vol. 188, art. no. 115945, 2019, doi: 10.1016/j.energy.2019.115945.
[24] M.Z. Sogut, "Assessment of small scale turbojet engine considering environmental and thermodynamics performance for flight processes," Energy, vol. 200, art. no. 117226, 2020, doi: 10.1016/j.energy.2020.117226.
[25] H. Tuzcu, Y. Sohret, and H. Caliskan, "Energy, environment and enviroeconomic analyses and assessments of the turbofan engine used in aviation industry," Environmental Progress & Sustainable Energy, vol. 40, no. 3, art. no. e13547, 2021, doi: 10.1002/ep.13547.
[26] I. Yazar, E. Kiyak, and F. Caliskan, "Simulation-based dynamic model and speed controller design of a small-scale turbojet engine," Aircraft Engineering and Aerospace Technology, vol. 90, no. 5, pp. 731-738, 2018, doi: 10.1108/aeat-09-2016-0150.
[27] Y. Şöhret, "A comprehensive approach to understanding irreversibility in a turbojet," Propulsion and Power Research, vol. 7, no. 2, pp. 129-137, 2018, doi: 10.1016/j.jppr.2018.03.004..